

Structurally Conserved Nop56/58 N-terminal Domain Facilitates Archaeal Box C/D Ribonucleoprotein-guided Methyltransferase Activity^{*[5]}

Received for publication, November 17, 2011, and in revised form, March 27, 2012. Published, JBC Papers in Press, April 11, 2012, DOI 10.1074/jbc.M111.323253

Keith T. Gagnon¹, Shyamasri Biswas², Xinxin Zhang, Bernard A. Brown II, Paul Wollenzien, Carla Mattos, and E. Stuart Maxwell³

From the Department of Molecular and Structural Biochemistry, North Carolina State University, Raleigh, North Carolina 27695

Background: Box C/D RNPs direct site-specific 2'-O-methylation of rRNA.

Results: The Nop56/58 and fibrillarin core proteins establish a very stable dimer with Nop56/58 contributing to methyltransferase activity.

Conclusion: The Nop56/58 core protein plays a role not only in RNP assembly, but also methyltransferase activity.

Significance: Our observations reveal a novel role for the Nop56/58 core protein in box C/D RNP function.

Box C/D RNA-protein complexes (RNPs) guide the 2'-O-methylation of nucleotides in both archaeal and eukaryotic ribosomal RNAs. The archaeal box C/D and C'/D' RNP subcomplexes are each assembled with three sRNP core proteins. The archaeal Nop56/58 core protein mediates crucial protein-protein interactions required for both sRNP assembly and the methyltransferase reaction by bridging the L7Ae and fibrillarin core proteins. The interaction of *Methanocaldococcus jannaschii* (Mj) Nop56/58 with the methyltransferase fibrillarin has been investigated using site-directed mutagenesis of specific amino acids in the N-terminal domain of Nop56/58 that interacts with fibrillarin. Extensive mutagenesis revealed an unusually strong Nop56/58-fibrillarin interaction. Only deletion of the NTD itself prevented dimerization with fibrillarin. The extreme stability of the Nop56/58-fibrillarin heterodimer was confirmed in both chemical and thermal denaturation analyses. However, mutations that did not affect Nop56/58 binding to fibrillarin or sRNP assembly nevertheless disrupted sRNP-guided nucleotide modification, revealing a role for Nop56/58 in methyltransferase activity. This conclusion was supported with the cross-linking of Nop56/58 to the target RNA substrate. The Mj Nop56/58 NTD was further characterized by solving its three-dimensional crystal structure to a resolution of 1.7 Å. Despite low primary sequence conservation among the archaeal Nop56/58 homologs, the overall structure of the archaeal NTD domain is very well conserved. In conclusion, the archaeal Nop56/58 NTD exhibits a conserved domain structure whose

exceptionally stable interaction with fibrillarin plays a role in both RNP assembly and methyltransferase activity.

Eukaryotic small nucleolar RNAs (snoRNAs)⁴ guide the site-specific modification of ribonucleotides in target RNAs (1–4). The box C/D and H/ACA RNAs comprise the two major snoRNA families that guide 2'-O-methylation and pseudouridylation, respectively (1). Their primary target RNA for modification is ribosomal RNA but other target RNAs include the spliceosomal snRNAs and select mRNAs (5–7). SnoRNAs base pair with their target RNA to determine the specific nucleotide for modification with snoRNA-bound proteins catalyzing the modification reactions (4, 8). Homologous box C/D and H/ACA small RNAs (sRNAs) and RNA-protein complexes (sRNPs) guide the same nucleotide modification reactions in Archaea (8).

The archaeal box C/D sRNPs provide a model system for structural and functional studies because of their minimal size and their ability to be reconstituted *in vitro* as catalytically active complexes (9, 10). Archaeal box C/D sRNAs are 50–70 nucleotides in size and possess well conserved box C, C', D, and D' sequences (3, 4). Boxes C and D located at the 5' and 3' termini, respectively, base pair to form the box C/D motif folded into a kink-turn (K-turn) (11, 12). Internal boxes C' and D' base pair to form the C'/D' motif, which exhibits a variant of the K-turn known as the K-loop (10, 13). In Archaea, these two RNA motifs are bound by the box C/D core proteins to assemble the terminal box C/D and internal C'/D' RNPs. Target RNAs base pair with box C/D and C'/D' RNP-associated guide sequences to direct the 2'-O-methylation of specific nucleotides in the target RNA (2, 9). Importantly, the inter-RNP spacing of these two subcomplexes is highly conserved at 12 nucleotides and alteration of this distance disrupts sRNP-guided nucleotide methylation (14).

* This work was supported, in whole or in part, by National Institutes of Health Grants GM069699 (to B. A. B.) and 1F32HD060377-01A1 (to K. T. G.) and National Science Foundation Grant MCB 0543741 (to E. S. M.).

[5] This article contains supplemental Figs. S1–S3.

The atomic coordinates and structure factors (code 3T7Z) have been deposited in the Protein Data Bank, Research Collaboratory for Structural Bioinformatics, Rutgers University, New Brunswick, NJ (<http://www.rcsb.org/>).

¹ Present address: Depts. of Pharmacology and Biochemistry, University of Texas Southwestern Medical Center at Dallas, Dallas, TX 75390-9041.

² Present address: Dept. of Biochemistry & Molecular Biology, University of Florida, P. O. Box 100245, 1600 S.W. Archer Rd., Gainesville, FL 32601.

³ To whom correspondence should be addressed: 128 Polk Hall, Raleigh, NC 27695. Tel.: 919-515-5803; Fax: 919-515-2047; E-mail: stu_maxwell@ncsu.edu.

⁴ The abbreviations used are: snoRNA, small nucleolar RNA; RNP, ribonucleoprotein; Mj, *M. jannaschii*; DSC, differential scanning calorimetry; AdoMet, S-adenosylmethionine; Δ5aa, 5-amino acid deletion; NTD, N-terminal domain; CTD, C-terminal Nop domain; CC, coiled-coil domain; Af, *A. fulgidus*; Ss, *S. sulfataricus*; Pf, *P. furiosus*; Ni-NTA, nickel-nitrilotriacetic acid.

The terminal box C/D and internal C'/D' RNPs are each assembled with three core proteins (10, 15, 16). L7Ae initiates box C/D and C'/D' RNP assembly by binding the K-turn and K-loop motifs. These L7Ae-sRNA complexes then serve as a binding scaffold to recruit Nop56/58, which uses its C-terminal domain (CTD or Nop domain) to bind the L7Ae-sRNA complex (10, 16, 17). The methyltransferase fibrillarin is then recruited by interaction with the Nop56/58 N-terminal domain (NTD) (18, 19). The Nop56/58 central coiled-coil (CC) domain promotes self-dimerization of this core protein (19), which provides intra-RNP protein-protein contact in the monoparticle as well as inter-RNP interaction of the dimeric complex. Thus Nop56/58 serves as a bridge between L7Ae and fibrillarin in both box C/D and C'/D' RNP assembly as well as linking these two subcomplexes in monomeric and dimeric sRNPs (15, 16, 20).

Core protein-protein interactions play critical roles in both box C/D sRNP assembly and the methyltransferase reaction. Crystal structures of each of the three core proteins as well as various protein-protein and RNA-protein complexes have revealed the basic structure of this RNP enzyme (16, 17, 21). Although it is clear that fibrillarin is the methyltransferase enzyme that binds the S-adenosylmethionine and the target RNA substrates, it is not yet understood how the L7Ae and Nop56/58 core proteins contribute to or even facilitate catalytic activity. The interaction of Nop56/58 with fibrillarin has now been investigated using site-directed mutagenesis of the Nop56/58 NTD. Nop56/58-fibrillarin dimerization is remarkably stable and not easily disrupted. Interestingly, however, two NTD mutations that did not affect RNP assembly nevertheless greatly reduced or abolished methyltransferase activity, indicating the importance of Nop56/58 for the 2'-O-methylation reaction. Supporting this functional contribution, Nop56/58 can be cross-linked to the target RNA. Determination of the *Methanocaldococcus jannaschii* (Mj) NTD crystal structure revealed that this domain is structurally well conserved among archaeal Nop56/58 homologs despite low sequence homology. Thus, the structurally conserved Nop56/58 NTD interacts with fibrillarin to play a role in not only box C/D sRNP assembly but also sRNP-guided nucleotide methylation.

EXPERIMENTAL PROCEDURES

RNA Synthesis and Radiolabeling—sR8 box C/D sRNA was transcribed and gel purified as previously described (10). Target RNA substrates were purchased from Integrated DNA Technologies (IDT). The 4-thiouridine-substituted D target RNA (5'-GA(s⁴U)CAUGCUCUAACGGUAGUAG-3') was purchased from Dharmacon. RNAs were 5'-terminal radiolabeled with ³²P as previously described (18).

Protein Expression and Purification—The *M. jannaschii* (Mj) L7Ae, fibrillarin, and Nop56/58 genes were cloned as previously described (10). L7Ae and fibrillarin were expressed with N-terminal His₆ tags and the Nop56/58 wild-type and mutant proteins were either N-terminal His₆ tagged or untagged. Protein genes were cloned into either pET21a or pET28a vectors (Novagen) and mutations were introduced using the Stratagene QuikChange site-directed mutagenesis kit. Deletions or truncations were generated by PCR amplification from existing

plasmids followed by subcloning into new pET28a vectors. The Nop56/58 coiled-coil deletion (Δ CC) was generated as previously described (20). All mutations, deletions, or truncations were verified by sequencing. Fibrillarin and L7Ae protein expression was induced in Rosetta DE3 cells (Novagen) using 1 mM isopropyl 1-thio- β -D-galactopyranoside and grown for 3 h at 37 °C. For production of Nop56/58 and its mutant proteins, expression was induced in Rosetta DE3 cells with 0.2 mM isopropyl 1-thio- β -D-galactopyranoside and grown for 24 h at 15 °C. Recombinant proteins were purified by Ni-NTA affinity chromatography or cation-exchange chromatography as previously described (10, 18). Prepared proteins were dialyzed against Buffer D (20 mM HEPES, pH 7.2, 3 mM MgCl₂, 100 mM NaCl, 0.2 mM EDTA, 0.5 mM DTT, 20% glycerol) and stored at -80 °C. N-terminal His₆ tags were removed by digestion with bovine thrombin before or during dialysis when desired (10).

Protein and RNP Affinity Co-purification and Nucleotide 2'-O-Methylation Activity Assays—Nop56/58-fibrillarin interaction was assessed via affinity purification or pulldown experiments examining dimer formation similar to that previously described (18, 20). Histidine-tagged fibrillarin was incubated at a 1:1 molar ratio with wild-type or mutant Nop56/58 protein in 1× HBSM buffer (20 mM HEPES, pH 7.4, 150 mM NaCl, 1 mM MgCl₂) at 70 °C for 5 min, followed by cooling to room temperature and a brief centrifugation to remove precipitated protein. Soluble protein was incubated for 15 min at room temperature with Ni-NTA resin equilibrated in Buffer D containing 50 mM imidazole. Ni-NTA resin was then washed (3 times) with Buffer D supplemented with 0.02% SDS and 0.1% Triton X-100. Bound protein was eluted in Buffer D containing 250 mM imidazole and then precipitated with 4 volumes of acetone. Dried protein pellets were resuspended in SDS sample buffer and resolved on 12% SDS-polyacrylamide gels.

sRNP assembly and assessment of *in vitro* 2'-O-methylation activity were accomplished as previously described (10). sRNP assembly for affinity purification of the complex was carried out using histidine-tagged wild-type L7Ae mixed with equimolar concentrations of untagged fibrillarin and untagged wild-type and mutant Nop56/58 proteins and incubated with a half-molar equivalent of 5'-radiolabeled sR8 sRNA. sRNP complexes were assembled at 70 °C for 10 min in 1× HBSM-300 (HBSM with a final NaCl concentration of 300 mM). Assembled complexes were purified by Ni-NTA chromatography as described above but in HBSM-300 buffer. Samples were resolved by SDS-polyacrylamide gel electrophoresis and visualized by Coomassie Blue staining for protein and phosphorimaging for radiolabeled RNA. For *in vitro* 2'-O-methylation assays, time points at 0 and 60 min were evaluated in triplicate and the mean \pm S.E. determined.

Differential Scanning Calorimetry (DSC)—DSC was performed using a MicroCal VP-DSC capillary cell microcalorimeter. Proteins were first dialyzed against 1× DSC buffer (10 mM cacodylate, pH 7.3, 250 mM NaCl, 250 mM KCl). Proteins at 25 or 50 μ M in degassed 1× DSC buffer were scanned under pressure from 35 to 125 °C at a scan rate of 90 °C/h. Temperatures corresponding to the maximum observed heat capacity (C_p) were designated the T_m (22). Average T_m values and S.D. were determined by statistical analysis of replicate scans.

prised of three structurally and functionally distinct domains (Fig. 1B) (17, 19). The C-terminal Nop domain (CTD) recognizes and binds the L7Ae core protein, which is the first core protein to bind the sRNA and initiate RNP assembly. The CC domain mediates self-dimerization of Nop56/58. This interaction couples the terminal box C/D and internal C'/D' RNPs in a monomeric sRNP (20) and is responsible for the formation of a dimeric sRNP complex (15). The NTD binds fibrillar and is responsible for heterodimer formation. In sRNP assembly, fibrillar is the last core protein added to the complex and is the methyltransferase enzyme that catalyzes the nucleotide modification reaction.

A number of site-specific mutations or deletions were incorporated into the NTD of *M. jannaschii* (*Mj*) Nop56/58. Although disruption of heterodimerization with fibrillar was the goal, mutants that would retain fibrillar binding but compromise box C/D sRNP activity were also sought. Computational alanine scanning of the archaeal Nop56/58-fibrillar crystal structure from *Archaeoglobus fulgidus* (*Af*) suggested specific amino acids for mutation that might weaken or disrupt *Mj* Nop56/58-fibrillar heterodimer formation (Fig. 2A) (19, 32). Initial alignment of the two archaeal Nop56/58 primary sequences indicated that the NTD is not highly conserved. Nevertheless, superimposition of available crystal structures of the Nop56/58-fibrillar heterodimer from *A. fulgidus* (*Af*), *Pyrococcus furiosus* (*Pf*), and *Sulfolobus sulfataricus* (*Ss*) revealed the overall conservation of the protein folded structure and the region of the NTD interface interaction with fibrillar (Fig. 2B).

Select mutations clustered around a hydrophobic region in the *Af*NTD crystal structure (corresponding to substitution of Tyr⁹ with a glycine, called Y9G, and a deletion of amino acids Ser⁶⁹, Thr⁷⁰, and Glu⁷¹, called ΔSTE, in the *Mj* Nop56/58 protein) that forms the interface with fibrillar. Additional mutations were made in the *Mj* Nop56/58 α-helix corresponding to *Af* helix 3 (α-3), which also contacts fibrillar. Mutations in helix α-3 included single substitutions (R100D and K112D), double substitutions (M103A/H104A and V114A/I115A), a quadruple substitution (M103A/H104A/V114A/I115A, called 4mut), as well as a deletion of the 5 amino acids Ser¹⁰⁷–Thr¹¹¹ (Δ5aa). Large domain deletions or truncations were also made in *Mj* Nop56/58 as controls. These were deletion of the Nop56/58 NTD domain (ΔNTD), the coiled-coil region (ΔCC), or the highly charged and poorly conserved C-terminal tail (ΔK-tail) (33, 34). Control constructs also included the individual NTD and CTD domains alone.

Interaction of the Nop56/58 mutants with fibrillar was assessed using co-precipitation or “pulldown” experiments (Fig. 2C). Recombinant N-terminal His-tagged fibrillar was incubated with the nontagged recombinant Nop56/58 mutants at 70 °C to encourage dimerization of these thermophilic proteins and then slowly cooled before mixing with charged Ni-NTA resin. After washing, bound protein was eluted with imidazole and resolved by SDS-polyacrylamide gel electrophoresis. Unexpectedly, all site-specific mutations in the *Mj* Nop56/58 NTD were still able to dimerize with fibrillar. Nop56/58 mutants where whole domains were deleted yielded the expected results. Only the Nop56/58 mutant lacking an

NTD was unable to bind fibrillar. (Control experiments lacking tagged fibrillar ensured that the Nop56/58 proteins were not binding nonspecifically to the resin, see supplemental Fig. S1.) These initial results indicated that Nop56/58-fibrillar dimerization is not easily disrupted by simple amino acid changes or small deletions in the Nop56/58 interface region.

Site-directed mutagenesis was consistent with a strong interaction between Nop56/58 and fibrillar that was resistant to numerous amino acid replacements and deletions. Previous examination of the *Af* Nop56/58-fibrillar crystal structure had suggested strong dimer stability based upon the largely nonpolar Nop56/58 NTD interface and high surface complementarity exhibited by these two proteins (19). To further investigate Nop56/58-fibrillar stability, the heterodimer was subjected to various chemical reagents known to weaken or disrupt protein-protein interactions (Fig. 3A). Again, pulldown experiments using His-tagged fibrillar assessed heterodimer stability. Dimers bound to the affinity column were washed with buffer containing high concentrations of salt (5 M NaCl), nonionic detergent (5% Triton X-100), or chaotropic agents (8 M urea or 6 M guanidine hydrochloride) before fibrillar elution with imidazole. Only the strong chaotropic agent guanidine hydrochloride was able to disrupt dimerization.

The melting temperature of fibrillar and select Nop56/58 proteins, either alone or when bound to fibrillar, was determined by DSC. DSC can melt samples under pressure, allowing scans at temperatures up to 130 °C. Changes in heat capacity (C_p) are recorded and the peak change in C_p indicates the T_m , or temperature at which half of the protein population is unfolded or melted (22). Both fibrillar and Nop56/58 proteins exhibited high unfolding temperatures with T_m values ranging from 85 to 98 °C. The Nop56/58 NTD itself was stable with a T_m of ~91 °C. Remarkably, dimerization of fibrillar with the Nop56/58 NTD resulted in a protein complex with an elevated T_m of ~113 °C (Fig. 3B). All tested Nop56/58-fibrillar dimers that contained an intact NTD yielded a similarly elevated T_m (Fig. 3C). In the case of the ΔK-tail and K112D Nop56/58 mutants, two other peaks in C_p beside that of the dimer were observed. These peaks appear to be free Nop56/58 or fibrillar proteins based on the temperature at their C_p maxima. However, the major peak always corresponded to the highest T_m value (supplemental Fig. S2). These observations revealed that the Nop56/58-fibrillar dimer exhibits an unusually stable protein-protein interaction.

Mutation of the Nop56/58 NTD Interface Does Not Disrupt sRNP Assembly But Can Impair Nucleotide Methylation—The methyltransferase fibrillar is the last protein added in RNP assembly and establishes a catalytically competent nucleotide methylation complex (9, 10, 19). This recruitment acts through direct fibrillar interaction with the NTD of Nop56/58. Nop56/58 is, in turn, bound to the L7Ae-sRNA complex through its C-terminal Nop domain (17, 19). The ability of *Mj* Nop56/58 NTD mutants to fully assemble complete box C/D sRNPs was assessed using pulldown experiments (Figs. 4, A and B). Radiolabeled *Mj* sR8 box C/D sRNA and *Mj* core proteins Nop56/58, fibrillar, and His-tagged L7Ae were used to assemble the sRNP complex. Analysis of the various Nop56/58 domain deletion mutants demonstrated, as anticipated from

Nop56/58 Facilitates Box C/D sRNP Activity

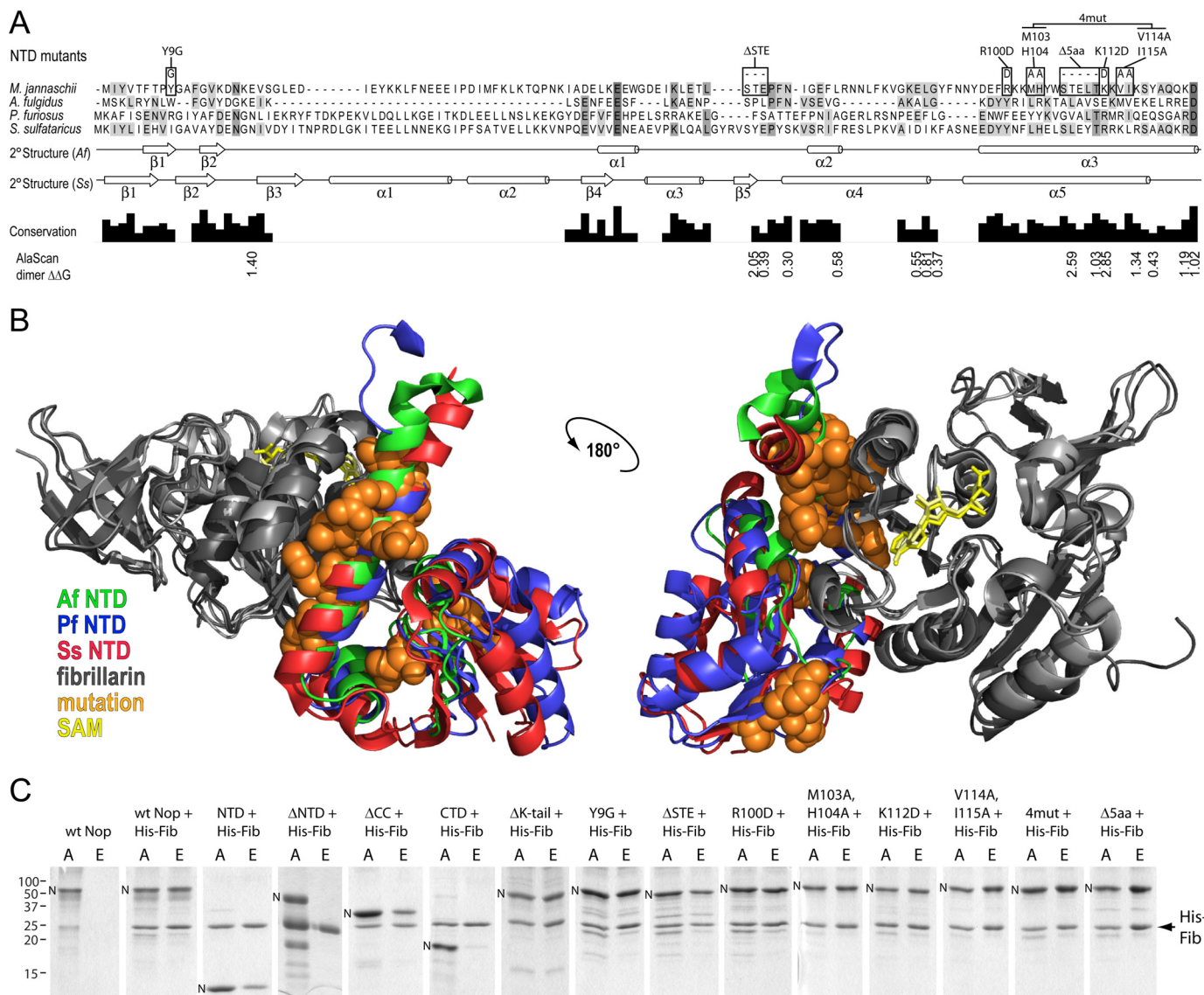


FIGURE 2. The NTD of Nop56/58 presents a well conserved interface for fibrillar dimerization that is not easily disrupted by mutagenesis. *A*, the NTD of the *M. jannaschii* Nop56/58 protein sequence aligned with the archaeal NTD sequence of *A. fulgidus*. Conserved (shaded dark gray) and similar (shaded light gray) amino acids are indicated. Point mutations and deletions of the *Mj* Nop56/58 NTD used in this investigation are indicated above the *Mj* NTD sequence. Computational alanine scanning scores above 0.25 used to predict disruption of the *Af* Nop56/58-fibrillar heterodimer are indicated below and aligned with respect to their *Af* residue. Secondary structural elements observed in the crystallized *Af* NTD are shown below. *B*, the NTD of Nop56/58 forms a conserved dimerization interface with fibrillar. Crystal structures of the fibrillar-Nop56/58 dimer from *S. sulfataricus* (*Ss*) (17), *P. furiosus* (*Pf*) (33), and *A. fulgidus* (*Af*) (19) are superimposed to reveal conserved protein folding and the dimerization interface. Amino acids that have been mutated or deleted, as indicated in panel *A*, are shown as orange spheres on the *Ss* NTD. The fibrillar proteins are gray, the *S*-adenosylmethionine (SAM) cofactor is yellow, the *Ss* NTD is red, the *Pf* NTD is blue, and the *Af* NTD is green. The same structural presentation is shown at the right rotated diagonally and 180°. *C*, a series of *M. jannaschii* Nop56/58 NTD amino acid mutations or deletions did not disrupt dimerization with fibrillar. Wild type (*wt*) or amino acid mutated/deleted *Mj* Nop56/58 NTD domains were incubated with His-tagged fibrillar and the protein dimers were isolated by affinity chromatography. Proteins applied (*A*) to the Ni-NTA resin were washed, bound proteins were eluted (*E*) with imidazole, and then resolved by SDS-polyacrylamide gel electrophoresis. The mutant NTD domains are indicated above the respective gel lanes. The various sized Nop56/58 NTDs, which can migrate at different positions are indicated by *N*. Δ NTD, N-terminal domain deletion; Δ CC, coiled-coil domain deletion; Δ K-tail, deletion of the variable C-terminal lysine tail; other mutations or deletions are as indicated in panel *A*.

the previous co-precipitation experiments shown in Fig. 2C, that assembly of a complete sRNP complex requires the Nop56/58 NTD (Fig. 4A). The Nop56/58 NTD alone (NTD) was not able to bind the assembling complex as it lacked the CTD domain critical for Nop56/58 interaction with L7Ae. The Nop56/58 CTD (CTD) did bind L7Ae although assembly of the sRNP was incomplete as this construct lacked the NTD for fibrillar binding. Similarly, deletion of the NTD from Nop56/58 (Δ NTD) disrupted sRNP assembly as fibrillar was again unable to bind the assembling complex. Deletion of either

the Δ CC or the highly charged Δ K-tail had no effect and allowed complete sRNP assembly. In agreement with Nop56/58-fibrillar pull-down experiments in Fig. 2C, the Nop56/58 NTD site-specific amino acid substitution and deletion mutants assembled complete sRNP complexes (Fig. 4B). Only the Δ 5aa, which likely shortens the α -4 helix that directly contacts fibrillar, showed a deficiency in sRNP assembly and reduced fibrillar binding. Thus, extensive mutagenesis of the Nop56/58 NTD did not prevent fibrillar binding and therefore box C/D sRNP assembly.

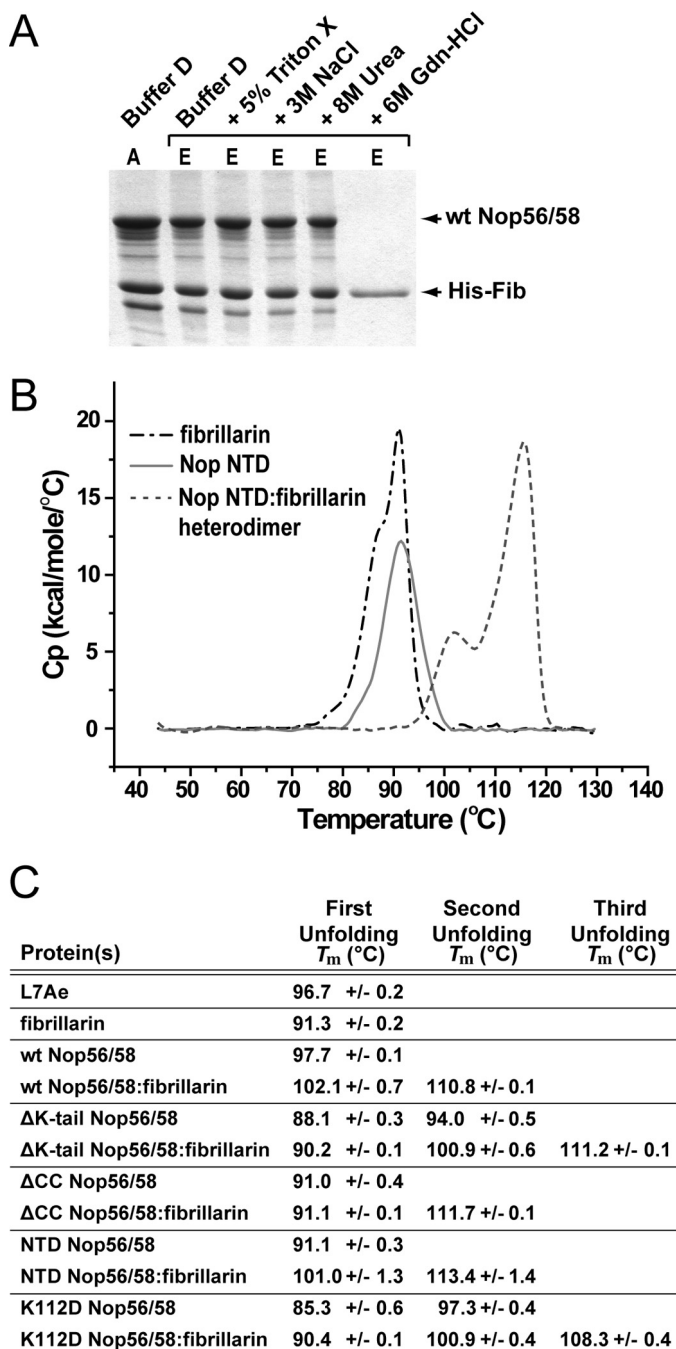


FIGURE 3. The archaeal box C/D sRNP Nop56/58 and fibrillarlin core proteins utilize an exceptionally stable interface for heterodimer formation. A, Nop56/58-fibrillarlin dimerization is maintained in the presence of strong chemical treatment. Nop56/58 was incubated with His-tagged fibrillarlin and the dimer was affinity selected using Ni-NTA resin. Protein dimers bound to the column were washed with buffer D (A, control) or buffer D containing reagents that disrupt protein-protein interactions, as indicated above the respective gel lanes (Triton X-100 nonionic detergent; NaCl; urea; Gdn-HCl (guanidine hydrochloride)). Bound proteins/dimers were then eluted (E) with imidazole and analyzed by SDS-polyacrylamide gel electrophoresis. B, the Nop56/58 NTD-fibrillarlin heterodimer exhibits increased thermal stability. DSC profiles of protein unfolding for 50 μ M of the Nop56/58 NTD, fibrillarlin, or the NTD-fibrillarlin heterodimer. C, summary of the differential scanning calorimetry of the individual box C/D sRNP core proteins and select Nop56/58 mutants alone or dimerized with fibrillarlin. Up to three peaks in heat capacity (C_p) were observed and are indicated as the first, second, or third protein unfolding T_m . Reported values are the average of two or more independent experiments with the S.D. indicated.

Subsequently, the ability of each of these sRNP complexes assembled with a mutated Nop56/58 core protein was investigated for sRNP-guided nucleotide 2'-O-methylation by measuring the incorporation of [3 H]CH $_3$ donated from S-adenosylmethionine (AdoMet) into target RNA substrates complementary to both the D and D' guide regions (9, 10). RNP assembly with individual NTD or CTD domains failed to guide nucleotide methylation, similar to complexes assembled with Nop56/58 missing either the NTD or coiled-coil domain. Previous work has shown that the coiled-coil domain is essential for sRNP-guided nucleotide methylation (20). Deletion of the C-terminal Nop56/58 lysine-rich tail (Δ K-tail) had no effect on either assembly or methyltransferase activity. Most amino acid and deletion mutants on the Nop56/58 interface had no effect upon methyltransferase activity, consistent with the assembly of a functional sRNP complex. However, two interface mutations did disrupt catalytic activity of the assembled complex. The single substitution K112D and the Δ 5aa deletion displayed significantly reduced and abolished activity, respectively. Although reduced methylation activity might be expected for the Δ 5aa deletion due to reduced fibrillarlin binding and sRNP assembly, the K112D single substitution showed no defects in fibrillarlin binding, heterodimer stability, or sRNP assembly.

Nop56/58 Cross-links with Target RNA Substrate—The possible interaction of the Nop56/58 core protein with the target RNA substrate was explored in UV cross-linking experiments where the target RNA possessed a site-specific 4-thiouridine (s^4 U) to enhance cross-linking efficiency and specificity. The s^4 U substitution was positioned just 5' to the region of sRNA-target RNA complementarity and therefore not involved in sRNA:target RNA base pairing (Fig. 5A) (35). This target RNA was 5'-radiolabeled and complementary to the D guide region of the sRNA. Assembled RNP complexes were incubated in the presence of radiolabeled s^4 U D target RNA and after UVA irradiation (>320 nm) (23) the sRNPs were disrupted with SDS and the proteins and RNA were resolved by SDS-polyacrylamide gel electrophoresis. The sRNP core proteins were visualized by Coomassie staining and the radiolabeled target RNA was visualized by phosphorimaging.

Superimposition of the stained protein and RNA phosphorimage revealed the formation of a specific radiolabeled product that migrated slightly slower than Nop56/58 indicating that this core protein was cross-linked to the s^4 U D target RNA (Fig. 5B). Increasing irradiation time resulted in correspondingly greater amounts of the cross-linked protein-RNA product. This cross-linked complex was not observed with simple Coomassie staining presumably due to the low sensitivity of Coomassie staining and the low efficiency of the UV cross-linking reaction. Control assembly reactions not irradiated or that were irradiated with a radiolabeled but unsubstituted D target RNA did not yield this radiolabeled protein. Competition with unlabeled or unsubstituted D target RNA reduced the amount of the cross-linked protein. A radiolabeled band appeared below fibrillarlin whenever the sR8 box C/D sRNA and the radiolabeled D target RNA, either s^4 U substituted or unsubstituted, were both present in the reaction. This band migrates at the size expected for an RNA duplex composed of base-paired sR8 and target RNA. Addition of D target RNA lacking an s^4 U substituent

Nop56/58 Facilitates Box C/D sRNP Activity

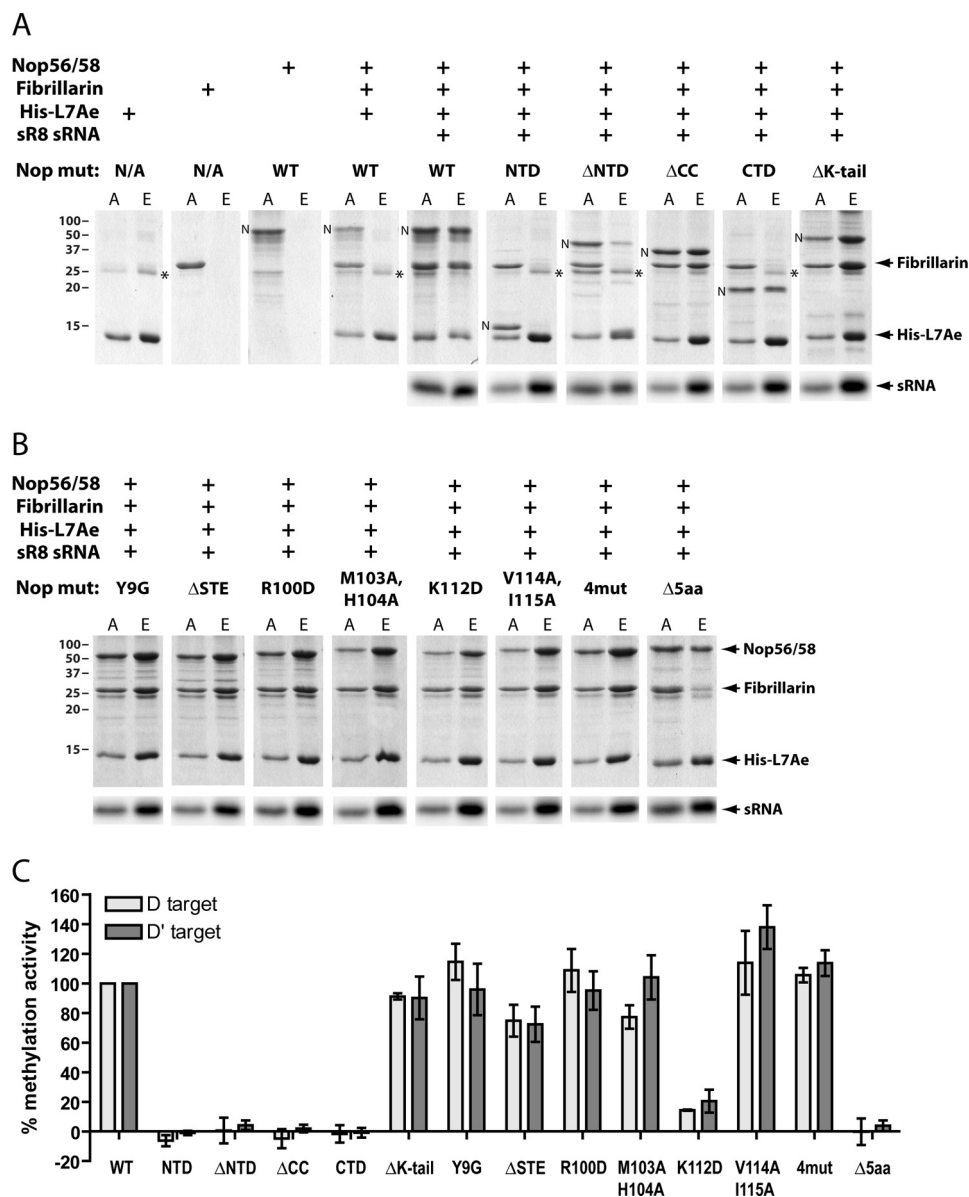


FIGURE 4. Alteration or deletion of Nop 56/58 NTD amino acids can disrupt box C/D sRNP-guided nucleotide 2'-O-methylation despite stable recruitment of the fibrillarin methyltransferase into the assembled complex. A and B, box C/D sRNP assembly with Nop56/58 mutants assessed by affinity co-purification of the RNP core components. His-tagged L7Ae, fibrillarin, 32 P-radiolabeled sR8 sRNA, and Nop56/58 mutants were incubated in the combinations indicated above each gel lane and the assembled complexes were applied (A) to Ni-NTA resin. After washing, bound complexes were eluted (E) and the RNP core proteins resolved on SDS-polyacrylamide gels. The mutant Nop56/58 proteins examined are listed above the respective gel lanes. RNP core proteins are indicated at the right and the bands corresponding to mutated Nop56/58 proteins in each lane are indicated by N. Asterisks indicate a nonspecific protein bands that co-purifies with His-tagged L7Ae and migrates just below fibrillarin. C, box C/D sRNPs assembled with an altered Nop56/58 core protein can affect sRNP-guided 2'-O-methylation of target RNA substrates. sRNP complexes were assembled with various mutant Nop56/58 core proteins and assayed for the ability of the terminal box C/D and internal C'/D' RNPs to guide nucleotide modification of their target RNA substrates. The deleted or mutated Nop56/58 core proteins used for sRNP assembly are indicated and the methyltransferase activity of the box C/D and C'/D' RNPs compared with wild type complex (wt).

tion produced a similar band but not the cross-linked protein migrating above Nop56/58. Unreacted, radiolabeled RNA migrated near the bottom of the gel below the L7Ae core protein.

Archaeal Nop56/58 N-Terminal Domain Exhibits a Conserved Folded Structure Despite Low Sequence Similarity Among Homologs—Alignment of the archaeal Nop56/58 and the eukaryotic Nop56 and Nop58 core proteins revealed that the N-terminal domain exhibits the lowest degree of conservation, whereas the coiled-coil and Nop domains are highly conserved (Fig. 2 and supplemental Fig. S3). Interestingly, existing

crystal structures of the archaeal Nop56/58 NTD from *S. sulfataricus* (*Ss*) and *P. furiosus* (*Pf*) reveal high structural similarity, even though the *Af*NTD exhibits fewer structural elements when compared with the *Ss* NTD (Fig. 2A). To determine whether low sequence but high structural conservation is a general feature of archaeal Nop56/58 NTDs, as well as to help interpret the mutagenesis experiments at a molecular level, the crystal structure of the *Mj* NTD was solved to 1.7 Å (Fig. 6 and Table 1). Initial attempts to solve the structure using the known structures of the archaeal Nop56/58 proteins (PDB codes 2NNW, 3ID5, and 1NT2)

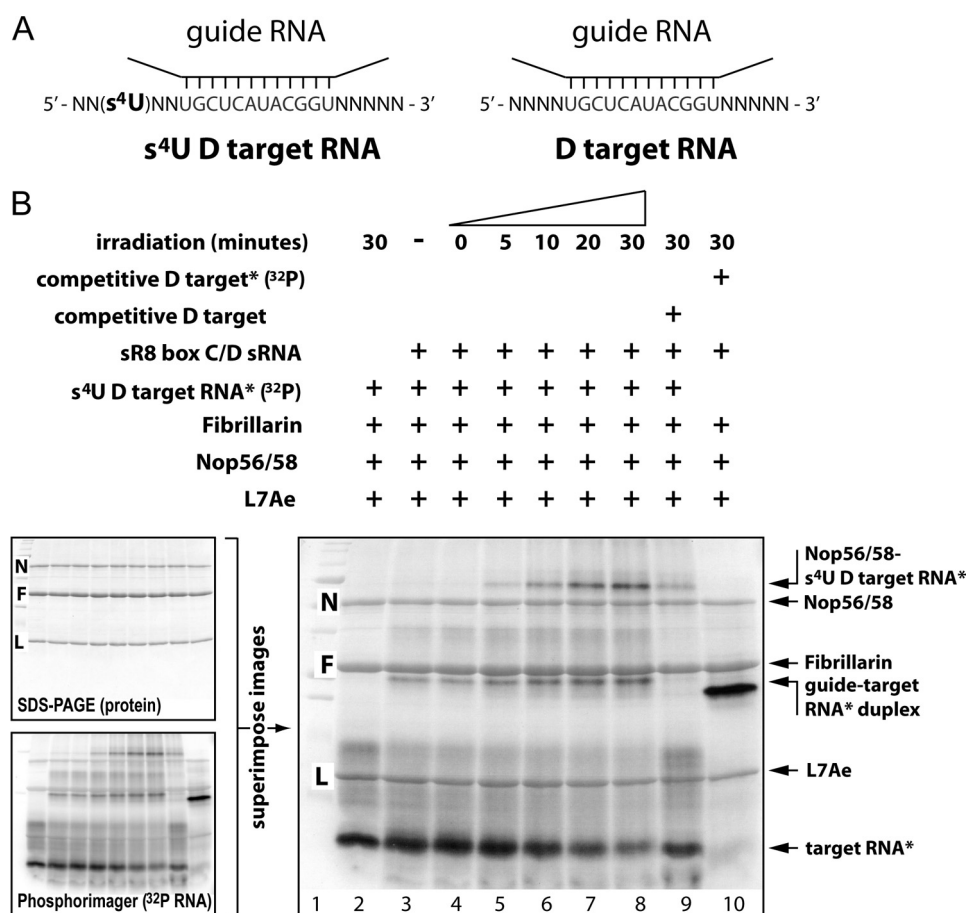


FIGURE 5. The box C/D sRNP target RNA cross-links to Nop56/58 in the assembled complex. *A*, schematic illustration of the D target RNA used for photocross-linking when base paired to the sR8 sRNA guide sequence. The position of the 4-thiouridine (s⁴U) substituted nucleotide within this target RNA is indicated. *B*, the target RNA substrate cross-links to the Nop56/58 core protein. Assembled box C/D sRNPs were incubated with radiolabeled target RNA and subsequently irradiated. The sRNP proteins and RNA were resolved by SDS-PAGE. Resolved proteins and radiolabeled RNA were visualized by Coomassie staining and phosphorimaging, respectively. Gel images of stained proteins and radiolabeled RNAs were superimposed to detect RNA cross-linked to proteins as revealed by shifted protein bands. Reaction components and treatments are indicated *above* the respective gel lanes and the identity of the RNA and protein bands are indicated on the *right*. *N*, *F*, and *L* designate the Nop56/58, fibrillarin, and L7Ae protein bands, respectively. An *asterisk* indicates the presence of radiolabeled target RNA.

failed due to the low sequence homology among them. However, using a selenomethionine-substituted *Mj* Nop56/58 protein successfully yielded a crystal whose structure was solved by single wavelength anomalous dispersion analysis. The *Mj* Nop56/58 N-terminal domain is composed of four β -sheets surrounded by four α -helices (Fig. 6, *A* and *B*). Two short 3_{10} helices are present between the β -2 and β -3 strands and at the N-terminal end of the α -3 helix.

Structural conservation analysis comparing the *Mj* and *Ss* Nop56/58 NTDs using Dali (36) yielded a high *Z*-score of 10 even though these two domains exhibited only 18% sequence identity. Similarly, comparison of the *Mj* NTD with the *Pf* and *Af* Nop NTD structures exhibiting 19 and 8% sequence identity yielded *Z*-scores of 8 and 3, respectively. Superimposed *Ss* and *Mj* NTD structures revealed similarly folded protein domains (Fig. 6, *C* and *D*). The C- α root mean square deviation values of *Mj* Nop56/58 NTD with that of *Ss* and *Pf* NTD structures was 1.9 Å, whereas the *Af* Nop NTD structure had a root mean square deviation value of 9.9 Å. Superimposing the *Mj* Nop56/58 NTD with other known archaeal Nop56/58 NTD structures revealed a well conserved three-dimensional fold overall (Fig. 7*A*). Of the four structures reported thus far, the *Af*

Nop56/58 NTD is the most divergent. The *Af* NTD has only 2 β -strands and 3 α -helices and the shortest N-terminal domain with 76 amino acid residues. In comparison, the *Mj* NTD is 121 residues and has 4 β -strands, 4 α -helices, and a 3_{10} helix and the *Pf* and *Ss* NTDs are 128 and 133 residues, respectively, with 5 β -strands and 5 α -helices each (Fig. 7*B*). Multiple sequence alignments combined with overlay of known Nop56/58 NTD-fibrillarin structures revealed that the Nop56/58 α -4 helix (α -3 helix in the *Af* structure), which mediates fibrillarin dimerization, is well conserved across Archaea (Figs. 2*B*, 6, *C* and *D*, and 7). It is predicted that the structure of the *Mj* fibrillarin-Nop56/58 heterodimer, as well as analogous heterodimers in other archaeal organisms, should conform to this conserved interaction. These results indicate a considerable amount of similarity in the folding of the N-terminal domain despite their very low primary sequence conservation.

DISCUSSION

Nop56/58 is one of three essential core proteins used to assemble the archaeal box C/D RNP nucleotide methylation complex. Nop56/58 plays a bridging role in RNP assembly using its C-terminal domain to bind the L7Ae-sRNA complex and

Nop56/58 Facilitates Box C/D sRNP Activity

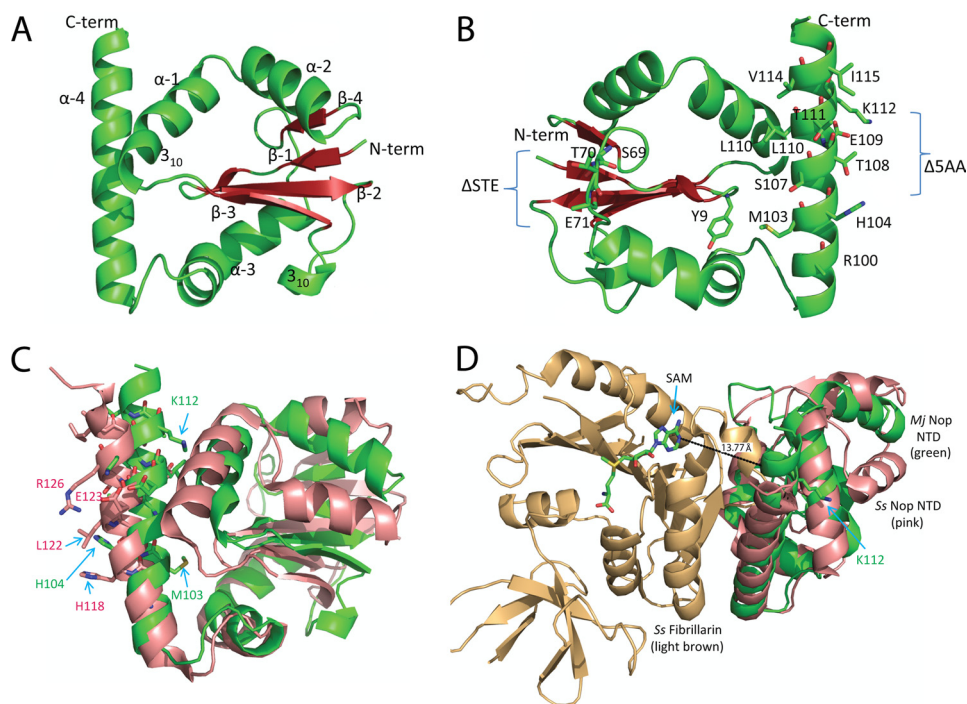


FIGURE 6. The crystal structure of the *M. jannaschii* Nop56/58 NTD reveals the spatial position of amino acid changes and their potential effect on the methyltransferase reaction. A, crystal structure of the *Mj* Nop56/58 NTD with its secondary structural elements indicated. The internal β -sheet is shown in red and the α -helices are shown in green. B, crystal structure of the *Mj* Nop56/58 NTD rotated 180° with mutated amino acids indicated (see Fig. 2A). C, superimposed Nop56/58 NTD structures of *Mj* in green and *S. sulfataricus* (*Ss*) in pink (17). Select amino acids of each NTD are indicated. D, superimposed *Mj* Nop56/58 NTD (green) with *Ss* Nop56/58 NTD-fibrillarilin dimer (pink and light brown). The *Mj* K112 amino acid and AdoMet cofactor bound to the *Ss* fibrillarilin protein are indicated. The distance between *Ss* α -helix 4 and AdoMet molecule was calculated at 13.77 Å and is indicated by a black dotted line.

TABLE 1
Crystallographic data

	Selenomethionine	Native
Space group	F222	F222
Cell dimensions:		
a, b, c (Å)	45.95, 88.03, 129.43	45.695, 86.511, 129.387
α, β, γ (°)	90, 90, 90	90, 90, 90
Resolution (Å)	2Å	1.7Å
R_{merge} (%) ^b	6.20% (25.5%) ^a	7.30% (37.6%) ^a
$I/\sigma I$	35.6 (4.3) ^a	38.4 (2.9) ^a
Redundancy	7 (4.2) ^a	5.8 (3.4) ^a
Completeness (%)	98% (84.5%) ^a	89% (38%) ^a
Reflections (Measured/Unique)	118013/16810	73723/12790
Phasing		
Number of sites	2 Se, 3 Zn	
Autosol BAYES-CC/FOM	46.4 ± 19.1 / 0.41	
Refinement		
Resolution		1.7Å-35Å
Number of reflections		12202
Rwork/Rfree		20.3/ 23.12
r.m.s.d		
Bond lengths (Å)/angles(°)		0.028/ 2.193
Number of residues/ion		
Protein		119
Water		70
Sodium		1
Ramachandran analysis		
Favoured/allowed/disallowed		117 / 2 / 0

^a Highest resolution bin.

^b $R_{\text{merge}} = \frac{\sum_{hkl} \sum_i |I_i(hkl) - \langle I(hkl) \rangle|}{\sum_{hkl} \sum_i I_i(hkl)}$, where $I(hkl)$ is the observed intensity of the i th measurement of reflection hkl and $\langle I(hkl) \rangle$ is the mean intensity of reflection hkl .

then its NTD to recruit the methyltransferase fibrillarilin. Examination of NTD interaction with fibrillarilin has revealed an exceptionally stable dimer. Mutagenesis of key amino acids on the NTD interface with fibrillarilin surprisingly did not block dimer formation. However, select mutations did affect the methyltransferase activity of the fibrillarilin. The cross-linking of Nop56/58 to the target RNA substrate further argued that this core protein is important for engaging the target RNA substrate for 2'-O-methylation. Determination of the *M. jannaschii* NTD crystal structure revealed that despite low sequence homology of this domain among archaeal homologs, all exhibit a well conserved folded structure. Thus, Nop56/58 mediates critical protein-protein interactions that are exceptionally stable, well conserved in the box C/D RNP scaffold, and important for both RNP assembly and methyltransferase function.

Mutagenesis of the Nop56/58 interface with fibrillarilin identified two alterations that were detrimental for methyltransferase activity, whereas having little or no effect upon sRNP assembly. Both the K112D substitution and the $\Delta 5aa$ are located near the center of the α -4 helix (α -3 in *Af*) of the *Mj* Nop56/58 NTD. The α -4 helix is ~14 Å from the fibrillarilin-bound AdoMet molecule (Fig. 6D). Thus, the α -4 helix is too distant from the fibrillarilin catalytic center to participate directly in the methyltransferase reaction.

The crystal structure of the *Mj* Nop56/58 NTD does predict that the $\Delta 5aa$ deletion mutant (STELT) would shorten helix 4 considerably, whereas the nearby K112D mutant would not be expected to significantly affect α -4 helix structure. Neither biochemical nor crystallographic analyses have provided clear

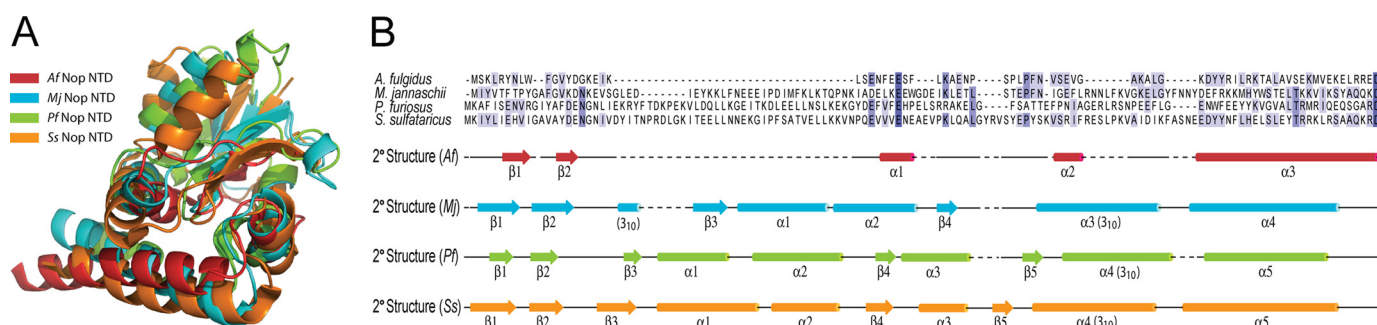


FIGURE 7. The archaeal Nop56/58 NTD is a structurally conserved domain. *A*, the archaeal Nop56/58 NTD possesses a conserved domain structure. Superimposed Nop56/58 NTD crystal structures of *M. jannaschii* (*Mj*), *S. sulfataricus* (*Ss*), *P. furiosus* (*Pf*), and *A. fulgidus* (*Af*). *B*, aligned NTD sequences and secondary structure elements of archaeal Nop56/58 proteins whose crystal structures have been solved. Conserved (shaded dark blue) and similar (shaded light blue) amino acids are indicated. Secondary structural elements observed in the crystallized Nop56/58 NTDs are illustrated below.

insight into how the mutated Lys¹¹² or STELT amino acids might facilitate the methyltransfer reaction. Lys¹¹² is a charged and highly conserved residue in both archaeal and eukaryotic Nop56/58 homologs (supplemental Fig. S3). In contrast, the nearby deleted STELT residues of the Δ5aa mutant are not particularly well conserved in sequence. Notably, however, both mutations either remove a positively charged amino acid (K112D) or alter the spatial positioning of a charged residue (the Lys/Arg residue C-terminal to the deleted STELT residues of Δ5aa) in α-4 helix. Perhaps this helix with its positively charged amino acids facilitates methyltransferase activity by interacting with the base-paired, guide-target RNA duplex, especially given its close proximity as revealed in a recent crystal structure of a fully assembled monomeric box C/D sRNP (16). The cross-linking of Nop56/58 to the target RNA substrate in the fully assembled sRNP complex is certainly consistent with this possibility.

Alternatively, the Nop56/58 NTD could mediate important but poorly understood sRNP dynamics and structural changes that take place prior to or during the methyltransfer reaction. Crystal structures have revealed that a linker between the Nop56/58 NTD and CC domain gives the NTD a high degree of flexibility (16, 17, 33). This flexibility may facilitate substrate binding and release by forming “open” and “closed” states. In the open state, fibrillarin and the Nop56/58 NTD would be distal to the guide RNA, thus allowing the substrate RNAs access to the guide sequences. In the closed state, fibrillarin would swing into close proximity to site specifically catalyze addition of a methyl group to the base-paired substrate RNA. Thus, the α-4 helix of Nop56/58 and the Nop56/58 interface with fibrillarin could play important roles in facilitating the dynamic nature of this sRNP. The K112D and Δ5aa deletion mutants could conceivably alter the α-4 helix structure to affect the dynamic nature of this domain and thus methyltransferase function.

The Nop56/58-fibrillarin heterodimer is a remarkably strong protein-protein interaction. This interaction was not disrupted by significant mutagenesis of the Nop56/58-fibrillarin interface, exhibits an exceptionally high melting temperature of ~113 °C, and was stable to all but the harshest of chemical treatments. Nop56/58 and fibrillarin are highly conserved proteins of both archaeal and eukaryotic organisms. Notably, however, there are two Nop56/58 homologs in eukaryotes that pre-

sumably arose from gene duplication (9, 10, 37, 38). Both Nop56 and Nop58 interact with fibrillarin in the eukaryotic box C/D snoRNP and both exhibit ~60% similarity with the *M. jannaschii* Nop56/58 protein (supplemental Fig. S3) (34). Sequence alignment of the archaeal and eukaryotic homologs reveals well conserved coiled-coil and CTD domains, both of which participate in important protein-protein interactions within the assembled RNP complex. Interestingly, the NTD is less conserved for the archaeal and eukaryotic homologs. Despite this weaker sequence conservation, crystal structures reveal a highly conserved domain structure. This is not surprising given the importance of this domain for interaction with fibrillarin and the ultimate assembly of a catalytically active box C/D RNP complex. Although crystal structures of eukaryotic Nop56 or Nop58 proteins are not yet available, it is highly probable that the N-terminal domains of both will exhibit conserved structures with respect to their archaeal homologs. These folded structures will clearly be critical for protein-protein interaction with fibrillarin and the bridging role that the Nop56 and Nop58 proteins most certainly play in eukaryotic snoRNP assembly. Our work here suggests that these interactions are not only important for assembly but also for efficient methyltransferase function as well. A better understanding of the structural dynamics of Nop56/58 within the box C/D RNP during multiple rounds of catalysis and the mechanistic details of how the NTD influences nucleotide methylation activity awaits further investigation.

Acknowledgments—We thank J. K. Watts and S. T. Younger for critical reading of the manuscript. We also thank members of the Dr. Rama Ranganathan laboratory for help with the differential scanning calorimetry experiments. We acknowledge members of beamline 22ID and 22BM APS Chicago for beam time assistance and Dr. Paul Schwartz (NCSSU) for remote data collection help.

REFERENCES

- Balakin, A. G., Smith, L., and Fournier, M. J. (1996) The RNA world of the nucleolus. Two major families of small RNAs defined by different box elements with related functions. *Cell* **86**, 823–834
- Kiss-László, Z., Henry, Y., Bachellerie, J. P., Caizergues-Ferrer, M., and Kiss, T. (1996) Site-specific ribose methylation of preribosomal RNA. A novel function for small nucleolar RNAs. *Cell* **85**, 1077–1088
- Omer, A. D., Lowe, T. M., Russell, A. G., Ehardt, H., Eddy, S. R., and Dennis, P. P. (2000) Homologs of small nucleolar RNAs in Archaea. *Sci-*

- ence **288**, 517–522
4. Gagnon, K. T., Zhang, X., and Maxwell, E. S. (2008) in *RNA and DNA Editing: Molecular Mechanisms and their Integration into Biological Systems* (Smith, H., ed) pp. 313–339, John Wiley and Sons, Inc., New York
 5. Darzacq, X., Jády, B. E., Verheggen, C., Kiss, A. M., Bertrand, E., and Kiss, T. (2002) Cajal body-specific small nuclear RNAs. A novel class of 2'-O-methylation and pseudouridylation guide RNAs. *EMBO J.* **21**, 2746–2756
 6. Kishore, S., and Stamm, S. (2006) The snoRNA HBII-52 regulates alternative splicing of the serotonin receptor 2C. *Science* **311**, 230–232
 7. Singh, S. K., Gurha, P., Tran, E. J., Maxwell, E. S., and Gupta, R. (2004) Sequential 2'-O-methylation of archaeal pre-tRNA^{Trp} nucleotides is guided by the intron-encoded but trans-acting box C/D ribonucleoprotein of pre-tRNA. *J. Biol. Chem.* **279**, 47661–47671
 8. Dennis, P. P., and Omer, A. (2005) Small noncoding RNAs in *Archaea*. *Curr. Opin. Microbiol.* **8**, 685–694
 9. Omer, A. D., Ziesche, S., Ebhardt, H., and Dennis, P. P. (2002) *In vitro* reconstitution and activity of a C/D box methylation guide ribonucleoprotein complex. *Proc. Natl. Acad. Sci. U.S.A.* **99**, 5289–5294
 10. Tran, E. J., Zhang, X., and Maxwell, E. S. (2003) Efficient RNA 2'-O-methylation requires juxtaposed and symmetrically assembled archaeal box C/D and C'/D' RNPs. *EMBO J.* **22**, 3930–3940
 11. Klein, D. J., Schmeing, T. M., Moore, P. B., and Steitz, T. A. (2001) The kink-turn. A new RNA secondary structure motif. *EMBO J.* **20**, 4214–4221
 12. Kuhn, J. F., Tran, E. J., and Maxwell, E. S. (2002) Archaeal ribosomal protein L7 is a functional homolog of the eukaryotic 15.5-kDa/Snu13p snoRNP core protein. *Nucleic Acids Res.* **30**, 931–941
 13. Nolivos, S., Carpousis, A. J., and Clouet-d'Orval, B. (2005) The K-loop, a general feature of the *Pyrococcus* C/D guide RNAs, is an RNA structural motif related to the K-turn. *Nucleic Acids Res.* **33**, 6507–6514
 14. Tran, E., Zhang, X., Lackey, L., and Maxwell, E. S. (2005) Conserved spacing between the box C/D and C'/D' RNPs of the archaeal box C/D sRNP complex is required for efficient 2'-O-methylation of target RNAs. *RNA* **11**, 285–293
 15. Bleichert, F., Gagnon, K. T., Brown, B. A., 2nd, Maxwell, E. S., Leschziner, A. E., Unger, V. M., and Baserga, S. J. (2009) A dimeric structure for archaeal box C/D small ribonucleoproteins. *Science* **325**, 1384–1387
 16. Lin, J., Lai, S., Jia, R., Xu, A., Zhang, L., Lu, J., and Ye, K. (2011) Structural basis for site-specific ribose methylation by box C/D RNA protein complexes. *Nature* **469**, 559–563
 17. Ye, K., Jia, R., Lin, J., Ju, M., Peng, J., Xu, A., and Zhang, L. (2009) Structural organization of box C/D RNA-guided RNA methyltransferase. *Proc. Natl. Acad. Sci., U.S.A.* **106**, 13808–13813
 18. Gagnon, K. T., Zhang, X., Agris, P. F., and Maxwell, E. S. (2006) Assembly of the archaeal box C/D sRNP can occur via alternative pathways and requires temperature-facilitated sRNA remodeling. *J. Mol. Biol.* **362**, 1025–1042
 19. Aittaleb, M., Rashid, R., Chen, Q., Palmer, J. R., Daniels, C. J., and Li, H. (2003) Structure and function of archaeal box C/D sRNP core proteins. *Nat. Struct. Biol.* **10**, 256–263
 20. Zhang, X., Champion, E. A., Tran, E. J., Brown, B. A., 2nd, Baserga, S. J., and Maxwell, E. S. (2006) The coiled-coil domain of the Nop56/58 core protein is dispensable for sRNP assembly but is critical for archaeal box C/D sRNP-guided nucleotide methylation. *RNA* **12**, 1092–1103
 21. Xue, S., Wang, R., Yang, F., Terns, R. M., Terns, M. P., Zhang, X., Maxwell, E. S., and Li, H. (2010) Structural basis for substrate placement by an archaeal box C/D ribonucleoprotein particle. *Mol. Cell* **39**, 939–949
 22. Gagnon, K. T., Pendergraft, H. M., Deleavey, G. F., Swayze, E. E., Potier, P., Randolph, J., Roesch, E. B., Chattopadhyaya, J., Damha, M. J., Bennett, C. F., Montallier, C., Lemaitre, M., and Corey, D. R. (2010) Allele-selective inhibition of mutant huntingtin expression with antisense oligonucleotides targeting the expanded CAG repeat. *Biochemistry* **49**, 10166–10178
 23. Nanda, K., and Wollenzien, P. (2004) Pattern of 4-thiouridine-induced cross-linking in 16 S ribosomal RNA in the *Escherichia coli* 30S subunit. *Biochemistry* **43**, 8923–8934
 24. Van Duyne, G. D., Standaert, R. F., Karplus, P. A., Schreiber, S. L., and Clardy, J. (1993) Atomic structures of the human immunophilin FKBP-12 complexes with FK506 and rapamycin. *J. Mol. Biol.* **229**, 105–124
 25. Otwinowsky, Z., and Minor, W. (1997) Processing of x-ray diffraction data collected in oscillation mode. *Methods Enzymol.* **276**, 307–326
 26. Adams, P. D., Afonine, P. V., Bunkóczi, G., Chen, V. B., Davis, I. W., Echols, N., Headd, J. J., Hung, L. W., Kapral, G. J., Grosse-Kunstleve, R. W., McCoy, A. J., Moriarty, N. W., Oeffner, R., Read, R. J., Richardson, D. C., Richardson, J. S., Terwilliger, T. C., and Zwart, P. H. (2010) PHENIX. A comprehensive Python-based system for macromolecular structure solution. *Acta Crystallogr. D Biol. Crystallogr.* **66**, 213–221
 27. McCoy, A. J., Grosse-Kunstleve, R. W., Adams, P. D., Winn, M. D., Storoni, L. C., and Read, R. J. (2007) Phaser crystallographic software. *J. Appl. Crystallogr.* **40**, 658–674
 28. Emsley, P., Lohkamp, B., Scott, W. G., and Kowtan, K. (2004) Features and development of Coot. *Acta Crystallogr.* **66**, 486–501
 29. Laskowski, R. A., MacArthur, M. W., Moss, D. S., and Thornton, J. M. (1993) Procheck. A program to check stereochemical quality of protein structures. *J. Appl. Crystallogr.* **26**, 283–291
 30. Davis, I. W., Leaver-Fay, A., Chen, V. B., Block, J. N., Kapral, G. J., Wang, X., Murray, L. W., Arendall, W. B., 3rd, Snoeyink, J., Richardson, J. S., and Richardson, D. C. (2007) MolProbity, all-atom contacts and structure validation for proteins and nucleic acids. *Nucleic Acids Res.* **35**, W375–W383
 31. Kleywegt, G. J. (1999) Experimental assessment of differences between related protein crystal structures. *Acta Crystallogr. D Biol. Crystallogr.* **55**, 1878–1884
 32. Kortemme, T., and Baker, D. (2002) A simple physical model for binding energy hot spots in protein-protein complexes. *Proc. Natl. Acad. Sci. U.S.A.* **99**, 14116–14121
 33. Oruganti, S., Zhang, Y., Li, H., Robinson, H., Terns, M. P., Terns, R. M., Yang, W., and Li, H. (2007) Alternative conformations of the archaeal Nop56/58-fibrillar complex imply flexibility in box C/D RNPs. *J. Mol. Biol.* **371**, 1141–1150
 34. Gautier, T., Bergès, T., Tollervey, D., and Hurt, E. (1997) Nucleolar KKE/D repeat proteins Nop56p and Nop58p interact with Nop1p and are required for ribosome biogenesis. *Mol. Cell. Biol.* **17**, 7088–7098
 35. Appel, C. D., and Maxwell, E. S. (2007) Structural features of the guide: target RNA duplex required for archaeal box C/D sRNA-guided nucleotide 2'-O-methylation. *RNA* **13**, 899–911
 36. Holm, L., and Park, J. (2000) DaliLite workbench for protein structure comparison. *Bioinformatics* **16**, 566–567
 37. Newman, D. R., Kuhn, J. F., Shanab, G. M., and Maxwell, E. S. (2000) Box C/D snoRNA-associated proteins. Two pairs of evolutionarily ancient proteins and possible links to replication and transcription. *RNA* **6**, 861–879
 38. Tran, E., Brown, J., and Maxwell, E. S. (2004) Evolutionary origins of the RNA-guided nucleotide-modification complexes. From the primitive translation apparatus? *Trends Biochem. Sci.* **29**, 343–350